Chemical Engineering Journal 146 (2009) 120–127

Contents lists available at ScienceDirect

Chemical Engineering Journal

journal homepage: www.elsevier.com/locate/cej

Kinetic modelling of methane decomposition in a tubular solar reactor

Sylvain Rodat[a,*], Stéphane Abanades[a], Julien Coulié[b], Gilles Flamant[a]

[a] Materials, and Solar Energy Laboratory, CNRS (PROMES-CNRS, UPR 8521), 7 Rue du Four Solaire, 66120 Odeillo Font-Romeu, France
[b] N-GHY Z.I. Montplaisir, Site Industriel St. Antoine, 51 rue Isaac Newton, 81000 Albi, France

ARTICLE INFO

Article history:
Received 17 June 2008
Received in revised form 2 September 2008
Accepted 3 September 2008

Keywords:
Methane cracking
Kinetic model
Plug-flow reactor
Hydrogen production
Solar reactor

ABSTRACT

Solar methane cracking is a promising pathway to produce hydrogen and carbon black with the bonus of zero CO_2 emission. A kinetic simulation of the methane decomposition in a tubular solar chemical reactor prototype is presented. This reactor is composed of four independent tubular reaction zones inserted in a graphite cavity receiver. Chemical reaction modelling is carried out thanks to the Dsmoke software, using a detailed kinetic scheme for the wide range modelling of alkane transformation. First, a kinetic analysis of the chemical system is presented to determine the sequence of methane cracking and a sensitivity analysis of the results on temperature (in the range 1500–2300 K) and on natural gas composition is performed. Then, a kinetic simulation of the solar reactor is proposed and implemented, in which each tubular reaction zone is modelled by three plug-flow reactors in series representing the pre-heating, isothermal, and cooling zones of the reactor. It predicts the evolution of gas species concentrations as a function of residence time. Comparisons with experimental results between 1670 K and 1770 K show good agreement for CH_4 conversion, and CH_4 and H_2 off-gas compositions.

1. Introduction

Special interest is given to the production of hydrogen as the future energy vector. Several H_2 production processes have reached maturity for commercial exploitation such as steam methane reforming (SMR), partial oxidation of heavy oils, catalytic decomposition of natural gas, and coal gasification, while other non-commercial H_2 sources are being developed such as methane pyrolysis, electrochemical processes, thermochemical water-splitting cycles, biomass gasification, and photo-biological processes [1]. Currently, hydrogen is mainly produced from fossil fuels and especially natural gas (consisting primarily of methane). These conventional processes lead to important CO_2 emissions. It was estimated that the global warming potential (GWP) of hydrogen production via the SMR process is 13.7 kg CO_2 (equiv.) per kg of H_2 produced (CO_2 accounts for 77.6% of the system's GWP) [2]. In order to avoid environmental impacts, new solutions are investigated. A promising one is the methane thermal dissociation [3–10] into hydrogen and carbon black (CB), two valuable products. If solar thermal power is used as energy input, no CO_2 emission occurs during the process. The overall reaction can be described as:

$$CH_4 \rightarrow 2H_2 + C \quad (1)$$

$\Delta H^\circ = 75\ \text{kJ mol}^{-1}$ ($216\ \text{kJ mol}^{-1}$ for CH_4 at 298 K and products at 2000 K)

Nevertheless, a more complex reaction scheme has to be used to explain the production of by-products such as C_2H_2, C_2H_4, and C_2H_6 and more complex molecules like polyaromatic hydrocarbons (PAHs). The kinetic mechanism can be described either as a simplified stepwise dehydrogenation: $2CH_4 \rightarrow C_2H_6 \rightarrow C_2H_4 \rightarrow C_2H_2 \rightarrow C$ [11] or as a more complex scheme including a free radical mechanisms composed of 36 and 119 reactions as proposed by Olsvik et al. [12] and Billaud et al. [13], respectively. A kinetic mechanism including only C_2H_2 as intermediate product was also reported [14]. A complete bibliographic survey concerning works on thermal decomposition of methane after 1960 was published by Billaud et al. [15]. Usually, the overall methane decomposition was considered of first order [6,16,17] but other orders were also reported. For example, Dahl et al. (2002) identified a reaction order of 4.4 [18,19]. This paper addresses a study on the kinetic scheme of methane decomposition reaction using the Dsmoke software and the comparison with experimental results obtained with a 10-kW tubular solar reactor. This reactor comprising a cavity-type receiver and four independent tubular reaction zones was developed to investigate natural gas cracking with a controlled temperature and with the possibility of scaling-up.

2. Description of the kinetic model

A kinetic software was used to predict the kinetics of natural gas cracking. The considered software called Dsmoke was devel-

* Corresponding author. Tel.: +33 4 68 30 77 31; fax: +33 4 68 30 29 40.
E-mail address: sylvain.rodat@promes.cnrs.fr (S. Rodat).

1385-8947/$ – see front matter © 2008 Elsevier B.V. All rights reserved.
doi:10.1016/j.cej.2008.09.008

oped by Faravelli and Ranzi at the Polytechnic University of Milan [20]. This software uses a detailed chemical kinetic scheme, with lumping procedures [21], for the modelling of alkane transformation for a wide composition range (from methane up to diesel fuel). It includes a detailed kinetic modelling of PAHs and soot formation. The high temperature mechanism for large PAHs and soot particles formation and growth is based on homogeneous reactions between gas phase species. More than 240 species and 14,000 reactions are implemented in Dsmoke code.

This model has been previously tested with respect to a very large set of experimental data for conditions that do not involve transport and diffusion processes, including plug-flow and stirred reactors, batch reactors and shock tubes, rapid compression machines and motored engines. It has been finally validated for a wide variety of chemical engineering problems, such as combustion, oxidative pyrolysis and steam cracking of alkane mixtures for application to future hypersonic propulsion [22] or for NO_x prediction in glass melting furnaces [23].

Using a sectional approach [24], PAHs composed of more than 20 carbon atoms and soot particles with diameters of up to 60 nm are divided into a limited number of classes covering different mass ranges. Each class is represented by a two or three lumped pseudo-species, called BIN, with a given number of carbon and hydrogen atoms [25]. The H/C ratio decreases with increasing molecular mass. BIN1 has 20 carbon atoms, and includes three different H/C ratios: 0.3, 0.5, and 0.8, so the species included in the model are BIN1A ($C_{20}H_{16}$), BIN1B ($C_{20}H_{10}$), and BIN1C ($C_{20}H_6$). BIN($n+1$) has twice the number of C atoms and mass range of BIN(n). This exponential sectional approach saves computation time while still maintaining a fair description of the low molecular weight components. For the smallest BINs, three different H/C ratios are selected (0.8, 0.5, and 0.3), while for larger BINs the selected level of H/C decreases in order to better match the overall dehydrogenation trend. The H/C ratios assigned to the last BINs are 0.2 and 0.05.

For this study, all BINs are considered as soot particles. The model permits to save data concerning a limited number of species (up to 30) even if much more species are computed. Thus, a limited number of the most relevant species was carefully selected: H_2, CH_4, BINs, PAHs: C_6H_6, C_8H_6, C_8H_8, C_9H_8, $C_{10}H_8$, $C_{12}H_8$, $C_{13}H_{10}$, $C_{14}H_{10}$, $C_{16}H_{10}$; non-methanic hydrocarbons (NMHCs): C_2H_2, C_2H_4, C_2H_6, C_3H_4, C_3H_6, C_3H_8, C_4H_2, C_4H_4 and free radicals: H, CH_3, C_3H_3. The kinetic model accounting for particle nucleation, formation of radicals, growth mechanisms of particles, oxidation mechanisms is fully described in Ref. [24]. The residence time is calculated for each iteration with the gas composition corresponding to the calculation step.

3. Kinetic analysis of the methane decomposition

Before modelling real experiments, a kinetic study of the methane decomposition was conducted. An isothermal plug-flow reactor at 101.325 kPa was assumed. Neither preheating of the reactants, nor cooling of the products was considered. Calculation results are presented as a function of residence time τ in the reactor (main variable). As a parametric analysis, the effects of reactor temperature and fuel composition are studied.

Performance criteria are reported in terms of:

CH_4 conversion:

$$X_{CH_4} = \frac{F_{0,CH_4} - F\ y_{CH_4}}{F_{0,CH_4}} \quad (2)$$

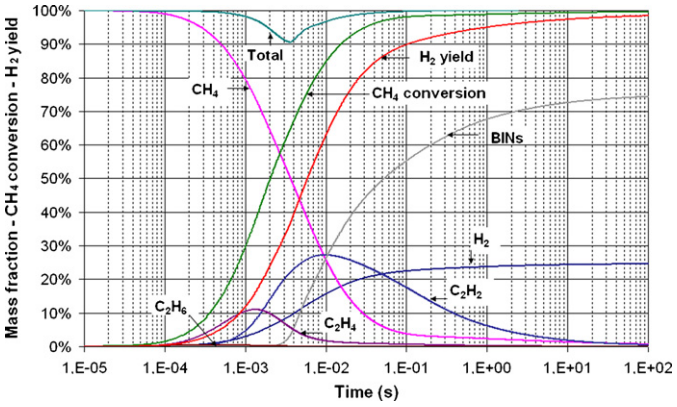

Fig. 1. Mass fractions, CH_4 conversion, and H_2 yield versus residence time at 1700 K.

H_2 yield:

$$Y_{H_2} = \frac{F\ y_{H_2}}{2F_{0,CH_4}} \quad (3)$$

where F_{0,CH_4} is the inlet molar flow-rate of CH_4, y_i is the mole fraction of species i, and F is the total outlet flow-rate (with argon as buffer gas) obtained from:

$$F = F_{Ar} + F\ y_{CH_4} + F\,y_{H_2} + F\,y_{C_2H_2} + F\,y_{C_2H_4} + F\,y_{C_2H_6} \quad (4)$$

3.1. Kinetic mechanism in an ideal isothermal reactor

The evolution of products mass fractions, CH_4 conversion, and H_2 yield as a function of residence time in an isothermal plug-flow reactor at 1700 K is given in Fig. 1. A gas feed composed of pure methane is considered. Residence time varies from 10^{-5} s to 100 s, which are extreme, non-realistic values, but this range is chosen in order to understand the kinetic mechanisms that are involved in H_2 and CB formation.

The total mass fraction is very close to 100% except for residence times between 0.3 ms and 30 ms. A total mass fraction near 100% means that the selected species are the only main compounds and that other side products are negligible. A total mass fraction lower than 100% means that side products, different from the selected ones, are also generated. It can be either PAHs that were not selected or other non-selected intermediate hydrocarbons. In this case, the real composition of the products should have to be checked more precisely and accurately. The mass fraction of hydrogen can increase up to 25%, which corresponds to the theoretical maximum value for complete dissociation of CH_4.

Concerning CH_4 conversion, it reaches 90% for a residence time of about 15 ms. A residence time longer than 100 ms is required in order to reach complete conversion. H_2 yield increases as soon as CH_4 conversion starts. H_2 yield strongly increases between 10^{-3} s and 10^{-1} s. A 90% yield is reached for a 100-ms residence time. Then for longer residence times, H_2 yield only slightly increases up to 100%. Increasing the residence time results firstly in the formation of C_2H_6, then C_2H_4 and C_2H_2 are produced. This scheme agrees with the successive dehydrogenation of CH_4 through C_2H_6, C_2H_4, and C_2H_2 proposed by Back and Back [11]. During these decompositions, the released hydrogen atoms create H_2. Next, C_2H_2 is used as the starting point for the growth of soots, and the release of H_2 on the other hand. Nevertheless, the simulation shows that additional compounds are involved in this mechanism since up to 10% of the total mass fraction is missing (between 3×10^{-4} s and 3×10^{-2} s) when only considering the selected species.

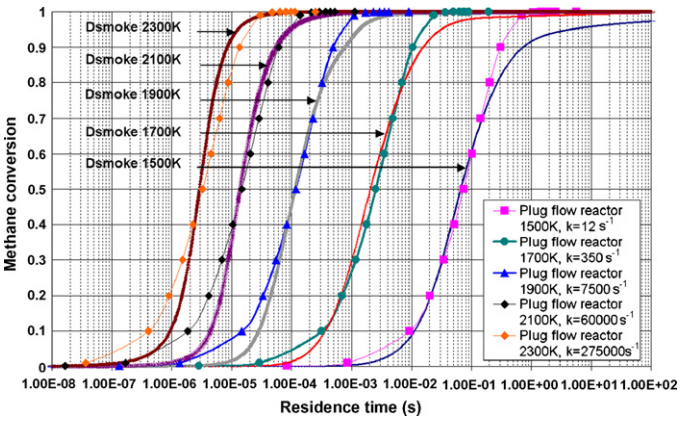

Fig. 2. Methane conversion versus residence time at different temperatures obtained from Dsmoke simulations and from a plug-flow reactor model.

This missing mass fraction mentioned above can also be observed for the other temperatures, the higher the temperature, the earlier the appearance of this missing mass fraction. As this result is an indication of the formation of intermediate hydrocarbon (HC) compounds, this means that the off-gas is "dirtier" at low temperature than at high temperature. For example, at 1500 K, intermediate HC compounds are formed between 10 ms and 0.3 s.

Despite CH_4 conversion significantly begins at $\tau = 10^{-4}$ s, soot formation only appears at $\tau > 2 \times 10^{-3}$ s. Soot formation increases markedly up to 1 s and increases slightly for larger τ. The maximum BINs mass fraction (75%, corresponding to the maximum carbon mass fraction that can be reached from complete CH_4 dissociation) would be ideally reached after 100 s. Soot mean diameter increases with the residence time to stabilize around 60 nm (the limit of the model) at large residence times.

3.2. Parametric analysis

A parametric analysis was carried out on temperature and natural gas composition.

Figs. 2 and 3 plot the CH_4 conversion and H_2 yield as a function of residence time for different temperatures ranging between 1500 K and 2300 K. Concerning CH_4 conversion, the higher the temperature, the lower the residence time required for the start of CH_4 dissociation (Fig. 2). Indeed, CH_4 dissociation starts from 5×10^{-4} s at 1500 K whereas it starts from 3×10^{-6} s at 1900 K. The same tendencies are observed on the H_2 yield versus residence time profiles (Fig. 3). However, for a temperature higher than 1900 K, a plateau

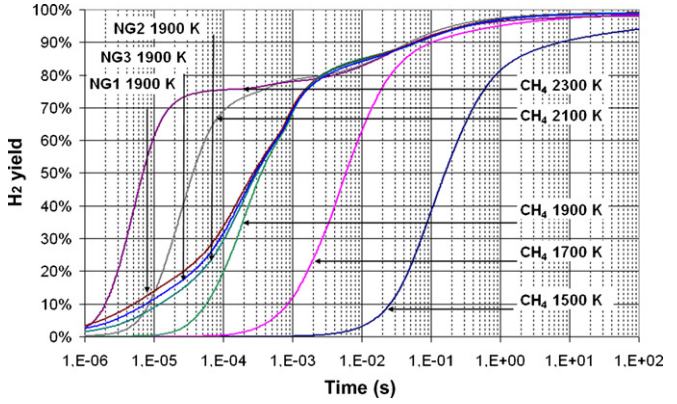

Fig. 3. Hydrogen yield versus residence time for different temperatures and natural gas compositions.

on the H_2 yield profiles is observed between 75% and 80% where H_2 yield grows up more slightly. This slow down in the H_2 yield rise mainly corresponds to unconverted C_2H_2. At 1500 K, the formation of H_2 is delayed and occurs for residence times longer than 1 ms; at this temperature, the final H_2 yield is lower than 95% because a complete conversion into H_2 cannot be reached even for the largest residence time considered.

The peaks of formation of all considered light HC compounds (C_2H_6, C_2H_4, C_2H_2 species) are shifted towards low residence times when the temperature increases. Nevertheless, it also appears that C_2H_2 is still unconverted after long residence times and that the level of remaining C_2H_2 is the most important at high temperatures (4% in mass after 10 s at 2300 K). As a result, increasing the temperature does not suppress the formation of secondary hydrocarbons.

BINs formation begins between 2×10^{-4} s (0.2 ms) for the highest temperature (2300 K) and 2×10^{-2} s (20 ms) for the coolest one (1500 K). For residence times higher than 20 ms, the evolutions of BINs mass fractions are very similar, except for the case at 1500 K where BINs formation begins later and BINs mass fraction does not reach 75% even after 100 s.

Based on the results presented in Fig. 2, the kinetic parameters for the global reaction of methane dissociation were identified with a simple reactor model. Assuming a first order kinetic expression [6,16,17] and an ideal plug-flow reactor model, the residence time τ can be calculated from [10]:

$$k\tau = -(1+\alpha)\beta \ln(1 - X_{CH_4}) - \alpha\beta X_{CH_4} \quad (5)$$

where α is the chemical expansion factor, β is the physical dilatation factor, and k is the kinetic rate constant, following an Arrhenius law:

$$k = k_0 \exp\left(\frac{-E_a}{RT}\right) \quad (6)$$

where E_a denotes the activation energy (J/mol), k_0 the pre-exponential factor (s^{-1}), R the universal gas constant (8.314 J/mol K), and T is the absolute temperature (K).

For each simulated temperature, it is possible to identify the kinetic rate constant k in Eq. (5) which best fits the Dsmoke simulation (Fig. 2). Then, from the plot $\ln(k) = f(1/T)$, a linear regression allows estimating a pre-exponential factor of $6.6 \times 10^{13}\ s^{-1}$ and an activation energy of 370 kJ/mol. The fair determination coefficient (0.9982) shows that the hypothesis of a first order reaction is adapted. These values of the kinetic parameters are in the range reported for a homogeneous (non-catalytic) methane decomposition reaction [26].

The model sensitivity on gas fuel composition at 1900 K is presented in Fig. 3 for three different natural gases and pure methane. Compositions of natural gases are given in Table 1. CH_4 conversion and H_2 yield show similar values whatever the gas composition for residence times higher than 1 ms. For residence times lower than 1 ms, CH_4 conversion and H_2 yield are better for natural gas than for pure methane due to the presence of ethane. Special care has to be taken if the natural gas contains CO_2 (NG3) since it is converted into CO, a highly toxic gas. For potential H_2 use in a polymer electrolyte membrane fuel cell (PEMFC), purification would be required

Table 1
Natural gas compositions

	Volume fractions (%)					
	CH_4	C_2H_6	C_3H_8	C_4H_{10}	CO_2	N_2
Methane (REF-G1)	100					
Modified algeria gas (NG1)	91.2	6.5	2.1	0.2		
Modified groningen gas (NG2)	83.5	4.7	0.7	0.2		10.8
North Sea gas (NG3)	88.2	5.4	1.2	0.4	1.4	3.2

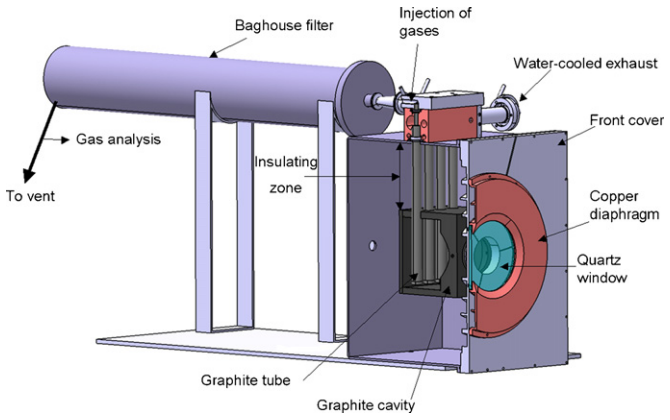

Fig. 4. Schematic configuration of the 10 kW solar reactor prototype.

to avoid the poisoning of the anode catalyst (usually based on platinum) by CO. The maximum tolerance on CO concentration for such application is 100 ppm [27].

4. Simulation of a tubular solar reactor

4.1. Reactor description

The reactor is presented in Fig. 4. It is composed of a 20-cm-side graphite cavity receiver (blackbody absorber of cubic shape). A 9-cm-diameter aperture lets concentrated solar radiation entering within the cavity through a quartz window. Thus, the inside cavity swept by nitrogen is separated from ambient oxidizing atmosphere. The reaction takes place in the four tubular graphite zones settled in parallel and vertically in the solar absorber. Each reaction zone, fed independently by a mixture of Ar and CH_4, is composed of two concentric graphite tubes: an inner tube for gas inlet (12 mm o.d., 4 mm i.d.) and an outer tube for gas outlet (24 mm o.d., 18 mm i.d.). The gas enters the inner tube and flows out by the annular space between the outer and inner tubes. The graphite tubes are heated up by both direct solar radiation coming from the aperture and by IR radiation from the cavity walls. The heated tube length inserted in the graphite cavity is about 0.161 m, the remaining length (about 0.203 m) corresponds to the insulation zone (Fig. 5). Three different insulating layers envelop the reactor cavity to lower conduction losses. It forms an insulation layer of 0.15 m (0.05 m for each insulating material). The three insulating materials are graphite felt in contact with the cavity ($\lambda = 0.46\,W\,m^{-1}\,K^{-1}$), an intermediate refractory ceramic fiber operating up to 1600 °C (62% Al_2O_3, 30% SiO_2, $\lambda = 0.35\,W\,m^{-1}\,K^{-1}$ at 1400 °C), and an outer microporous insulator operating up to 1000 °C (20% ZrO_2, 77.5% SiO_2, 2.5% CaO, $\lambda = 0.044\,W\,m^{-1}\,K^{-1}$ at 800 °C). The surrounding outer shell of the reactor is made of stainless steel (535 mm × 535 mm × 373 mm). The reactor is designed for a nominal power of 10 kW and it is set-up at the focus of the 1 MW solar furnace of CNRS-PROMES laboratory. The furnace is composed of a field of 63 heliostats for full power (45 m^2 per heliostat) and of a parabolic concentrator (1830 m^2) delivering up to 9000 suns at the focal plane. During experiments at 10 kW scale, only a fraction of the parabola is used by limiting the number of heliostats tracking the sun and by using a shutter.

4.2. Experimental procedure and results

The first experimental step was the heating of the reactor under an argon flow in the tubes. Once the desired temperature reached, the mixture of argon and methane was injected with a controlled

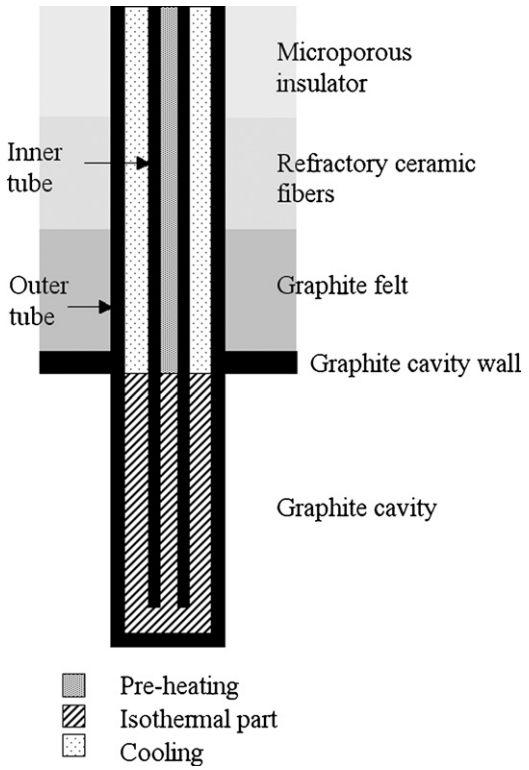

Fig. 5. Scheme of tube parts constituting the three plug-flow reactors.

composition. Two mass-flow meters were dedicated to each tube to control with accuracy the Ar and CH_4 flow-rates. The temperature was measured by a solar blind optical pyrometer (wavelength: 5.14 μm) pointing toward a graphite tube outer wall inside the cavity through a CaF_2 window and by a Pt–Rh thermocouple in contact with the graphite cavity wall. Since measurements showed that similar temperatures were reached by the tube wall and the graphite cavity wall (maximum discrepancy of 40 K), the temperature of the tubes inside the cavity was considered uniform [28].

At the exit of the four tubes, the exhaust gas–solid flows were collected and mixed together. The gas temperature was about 373 K, the products were cooled down and flowed through a filter bag to separate carbon particles. The pressure was monitored by pressure sensors placed at each tube entrance and was regulated thanks to the use of a vacuum pump. The filtered gas was then analysed to determine the gas composition. A continuous analyser permitted to monitor the concentration of H_2 and CH_4. The methods used for H_2 and CH_4 analysis were thermal conductivity and infrared detections, respectively.

A gas chromatograph also measured online the outlet concentration of CH_4, C_2H_6, C_2H_4, C_2H_2, and H_2. The chromatograph (Varian CP 4900) was equipped with two columns: MolSieve 5A PLOT for H_2 and CH_4, and PoraPLOT U for light hydrocarbons (C_2H_y). The chromatography analysis was based on thermal conductivity detection and the carrier gas was argon, also used as buffer gas during methane cracking experiments.

The main experimental conditions and corresponding results are listed in Table 2. Seventeen experimental tests were carried out. Temperatures varied between 1670 K and 1770 K and the CH_4 flow-rate in the feed varied between 1.2 L/min and 8 L/min (every volumetric gas flow-rates are given at normal conditions: 101.325 kPa and 273.15 K). CH_4 mole fraction was between 10% and 33%. The gas residence time ranged from 12 ms to 35 ms and it was calculated by dividing the volume of the tubular reaction zones

Table 2
Experimental conditions and corresponding results

	Ar (L/min)	CH_4 (L/min)	Pressure (Pa)	$T_{pyrometer}$ (K)	Residence time (s)	Off-gas (mole fractions)		
						H_2	CH_4	C_2H_2
1	10.8	1.2	40,000	1770	0.032	0.1625	0.0018	0.0202
2	16	4	38,000	1770	0.018	0.2518	0.0138	0.0392
3	16	4	35,000	1770	0.017	0.2555	0.0055	0.0417
4	20	4	35,000	1770	0.014	0.2170	0.0090	0.0302
5	16	4	32,000	1700	0.018	0.2056	0.0294	0.0398
6	16	6	35,000	1710	0.017	0.2925	0.0340	0.0530
7	16	6	25,000	1710	0.012	0.2278	0.0790	0.0361
8	10.8	1.2	30,000	1670	0.027	0.1033	0.0227	0.0207
9	16	8	30,000	1670	0.013	0.1230	0.2123	0.0179
10	18	2	30,000	1670	0.018	0.0795	0.0388	0.0160
11	16	4	30,000	1670	0.018	0.1480	0.0727	0.0282
12	14	6	30,000	1670	0.018	0.2270	0.1000	0.0426
13	18	2	30,000	1740	0.018	0.1177	0.0173	0.0258
14	16	4	30,000	1740	0.018	0.2173	0.0307	0.0448
15	14	6	30,000	1740	0.018	0.2943	0.0560	0.0536
16	24	6	30,000	1740	0.012	0.1617	0.0703	0.0264
17	8	2	30,000	1740	0.035	0.2523	0.0037	0.0187

inserted in the graphite cavity (isothermal zone in Fig. 5) by the total volumetric inlet gas flow-rate calculated at the actual tube temperature and pressure. This residence time assessment did not include the gas flow-rate expansion due to chemical reaction.

The gas-flow in the tubes was laminar with a Reynolds number smaller than 2000. The highest Reynolds number (1900) was obtained at the tube entrance. Then, it decreased with temperature because the gas kinematic viscosity increased faster than the gas velocity (gas feed: 4 L/min Ar and 1 L/min CH_4, pressure: 40 kPa, tube diameter: 4 mm, gas kinematic viscosity at 300 K: 3.87×10^{-5} m^2 s^{-1}).

The duration of an experiment was up to 1 h. Results did not depend on the experiment duration since steady state was rapidly reached. However, when the tubes started to block because of carbon deposition, the chemical conversion rate increased because the residence time increased. The experiment was then stopped.

The ratio between the carbon quantity exiting the reactor (weighted mass of solid carbon from the filter and the tubes, acetylene and residual methane from GC analysis) to the carbon quantity introduced (methane) was about 93%. The missing mass of carbon may be the non-removed carbon deposit in the tubes and the other undetected secondary hydrocarbons.

4.3. Model of the experimental reactor

The four tubes are identical since they are in parallel in an isothermal cavity. Moreover, the gas feed in each tube is independent and the same gas flow-rates are injected. Experiments also confirm that the conversion rate remains unchanged when stopping the gas feeding in one tube. Therefore, only one tube is considered in the kinetic simulations. When flowing in the tube, gases pass through two different zones consisting of a pre-heating zone, an isothermal zone, and a cooling zone. According to the tubular design of the reaction zones and to the laminar flow regime inside the tubes, a plug-flow is the most suitable assumption for the reactor model. Each tube is thus modelled by three plug-flow reactors in series (Fig. 5):

- *Pre-heating plug-flow reactor*: the temperature increases linearly from 300 K to the measured reactor temperature during the test. It corresponds to the part of the inner tube in the insulating layers. Since graphite has a much higher thermal conductivity than the insulating materials, the temperature gradient along the tube wall is directly connected to the thermal conductivity of graphite according to Fourier's law. Therefore, a linear temperature profile was chosen. This profile did not require any more adjustment because it did not affect the results at all. Indeed, simulation results showed that no reaction occurred in this pre-heating zone because both residence time and temperature were not high enough. It just allowed to increase the gas temperature and it was thus neglected in the kinetic simulations.

It was assumed that the gas temperature reached the reactor wall temperature at the exit of the pre-heating zone. Two parameters favor the gas pre-heating: first, the argon thermal conductivity is multiplied by 3 between 300 K and 1700 K, second, methane absorbs IR radiations. Besides, the start of the thermally developed region in the entrance region of a tube with constant wall temperature can be determined from [29]:

$$\frac{1}{Re\,Pr}\frac{x_d}{d} = 0.05$$

where Re is the Reynolds number, Pr is the Prandtl number, x_d is the start of the thermally developed region and d is the tube diameter.

From this correlation, x_d is about 28 cm for a wall temperature of 300 K and 10 cm for a wall temperature of 1700 K. Thus, the mean magnitude order for x_d corresponds roughly to the pre-heating zone length (20 cm).

- *Isothermal plug-flow reactor*: the temperature is set to the measured temperature of the reactor during the test. This zone of the tubes located in the cavity (thus receiving the solar irradiation) corresponds to the isothermal zone.
- *Cooling plug-flow reactor*: the temperature decreases from test temperature to 373 K. It corresponds to the annular space between the inner and the outer tube located in the insulating layers. This zone has been called "cooling zone" because it is not exposed to the solar irradiation and thus, the gas temperature decreases. Similarly to the pre-heating zone, the rate of temperature decrease in the cooling zone is linear.

For each simulated run, the experimental temperature and pressure used in the model are those specified in Table 2.

4.4. Simulation results and experimental validation

The kinetic model predictions concerning the gas composition as a function of residence time are given in Figs. 6 and 7 for experimental conditions 2 (temperature: 1770 K, CH_4 mole fraction: 20%).

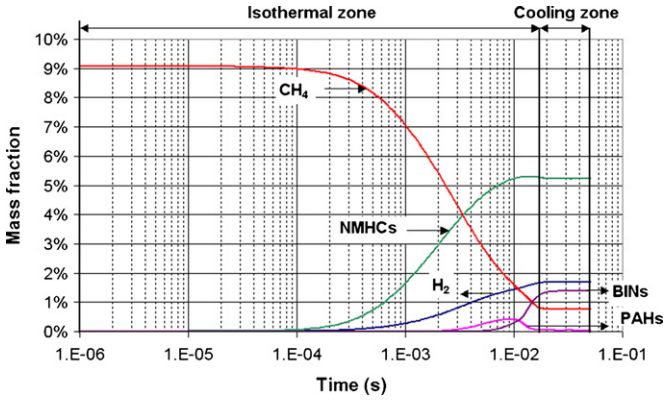

Fig. 6. Gas composition versus residence time from kinetic simulation of experimental condition 2.

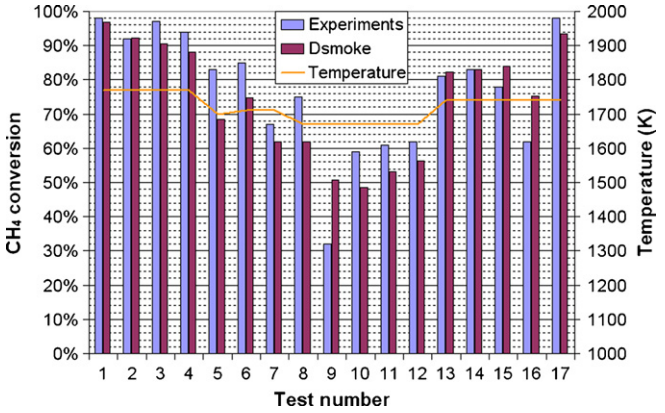

Fig. 8. Experimental and predicted methane conversions from the kinetic model for each experimental test.

As expected, the isothermal part is the key zone of the reactor: the conversion of methane and the production of hydrogen mainly occur in this zone as well as the non-simultaneous formation of NMHCs, PAHs, and BINs. Likewise, CB formation occurs later than H_2. These results are reported in Fig. 6 as a function of residence time, which was set to 0 at the entry of the isothermal zone. The residence time is about 17 ms in the isothermal zone and about 34 ms in the cooling zone. CH_4 starts to dissociate after 1×10^{-4} s. The formation of NMHCs (light hydrocarbons) is first observed followed by the formation of H_2. Then, PAHs and BINs are formed in a short residence time period. Actually, the decomposition of PAHs and the formation of CB just begin toward the exit of the isothermal zone for $\tau > 10$ ms.

Among NMHCs, C_2H_6 and C_2H_4 are the first species formed from CH_4 dissociation, as shown in Fig. 7. Both species are then converted into C_2H_2 with a nearly complete conversion at the exit of the isothermal zone ($\tau > 10$ ms). In the cooling zone, the CB formation slowly continues while C_2H_4 and C_2H_6 slightly increase presumably from C_2H_2 due to the temperature decrease. Predicted mole fractions of CH_4, H_2, and C_2H_2 at the reactor exit are 0.014, 0.248, and 0.056, respectively, which corresponds closely to the experimental values given in Table 2, except for C_2H_2.

Fig. 8 compares the CH_4 conversions obtained from kinetic simulations with Dsmoke code and from experiments. For most of the tests, experimental CH_4 conversion is higher than the simulated one but there is a reasonably good agreement between the two series (mean discrepancy of 12%). The carbon particles formed in the tubes may catalyse further the reaction. This catalytic effect is not included in Dsmoke software (homogeneous reaction), which may explain why the chemical conversions predicted by Dsmoke are usually lower than the experimental ones. The statement of homogeneous reaction considered by Dsmoke is consistent with the high value of activation energy (370 kJ/mol) identified from the plug-flow reactor model. In few cases (tests No. 9, 15, 16), the predicted CH_4 conversion is higher than the experimental one. This may be due to temperature measurement uncertainty. In some cases, especially at high CH_4 flow-rate in the feed, the gas temperature must be lower than the wall temperature measured by the pyrometer, due to the endothermic reaction. If the gas temperature is over-estimated, then the predicted conversion from Dsmoke simulation becomes higher than the experimental one. The influence of temperature is also clear: the higher the temperature, the higher the conversion, as shown in Fig. 8. The reaction of methane decomposition is endothermic; as a consequence, a temperature increase results in the reaction rate increase. According to thermodynamics [30], CH_4 decomposition is complete between 1273 K and 2273 K. Due to kinetic limitations, the experimental CH_4 conversions are not complete, which was expected since the residence time is too short to reach thermodynamic equilibrium. This influence of residence time on reaction extent is strong according to Dsmoke kinetic calculations.

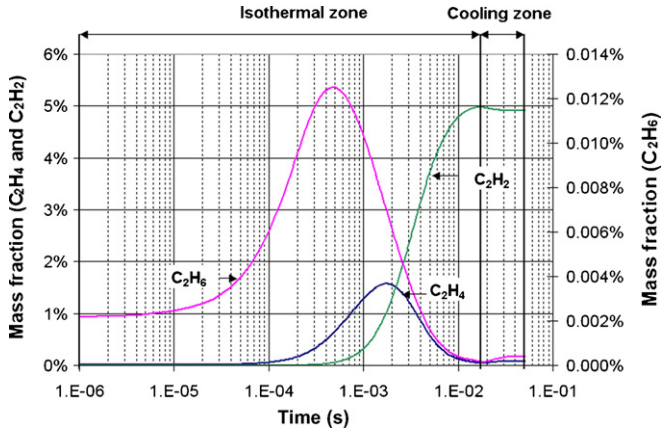

Fig. 7. C_2H_6, C_2H_4, and C_2H_2 mass fractions versus residence time from kinetic simulation of experimental condition 2.

Concerning the comparison between experimental and simulated H_2 yields, the mean discrepancy is 24%, which is not as good as for the CH_4 conversion. Experimental H_2 yield is always higher than the predicted one. Finally, Dsmoke always predicts higher off-gas C_2H_2 concentrations than the experimental ones (mean discrepancy of 32%), which explains the discrepancy on the H_2 yield. This disagreement with experiments may be due to the catalytic properties of CB reported previously [31] but that are not integrated in the Dsmoke model. An heterogeneous surface reaction may also occur on the tube walls, enhancing the dissociation reaction [32]. Concerning C_2H_4 and C_2H_6, their quantities in the gas products are not significant enough to conclude quantitatively but their concentrations tend to decrease when increasing the temperature.

The time evolution of H_2 and CH_4 mole fractions at 1740 K obtained from the model are reported in Figs. 9 and 10(lines) along with the experimental data corresponding to each experimental condition (marks). The slope breakage on lines takes place between the isothermal and the cooling zones and proves that a higher residence time in the isothermal zone (where the reaction rate is the highest) could lead to enhanced CH_4 conversion. At this transition point, the kinetic model gives the residence time of the gas in the isothermal zone, which corresponds roughly to that calculated without taking into account the chemical expansion (values given

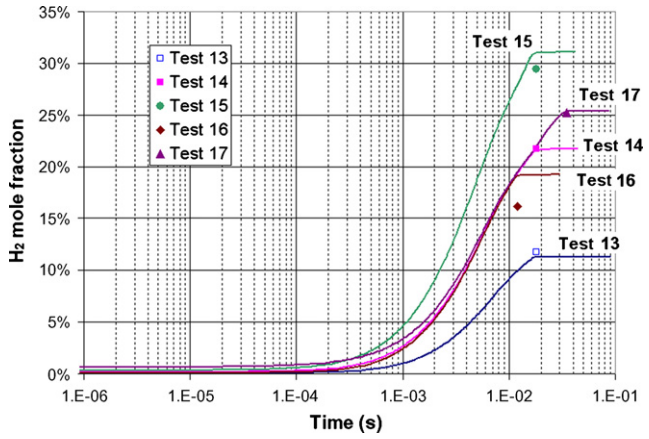

Fig. 9. Predicted H_2 mole fraction versus residence time and corresponding experimental data at 1740 K.

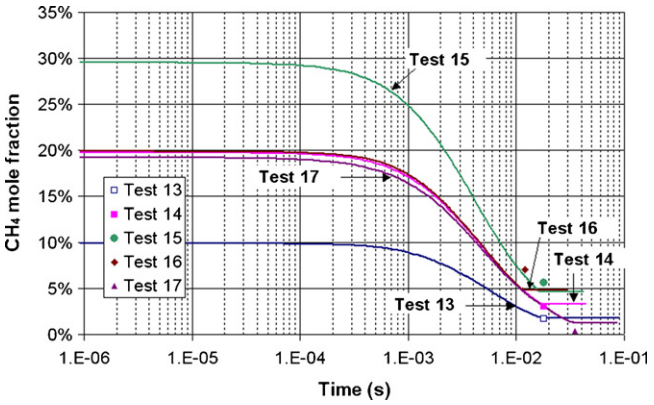

Fig. 10. Predicted CH_4 mole fraction versus residence time and corresponding experimental data at 1740 K.

in Table 2 for each experimental condition). Actually, the residence times obtained from the two different calculation methods (kinetic model and assessment from inlet gas-flow rate) are similar owing to the high dilution with argon. Moreover, simulated and experimental CH_4 and H_2 mole fractions are very comparable, which permits to validate the kinetic model applied to the solar process of methane cracking. On the basis of the results obtained with this 10 kW solar reactor, a pilot-scale solar reactor is being designed. To limit the carbon deposition issue, simple tubes will be preferred instead of concentric tubes. The graphite tubes could also be replaced by ceramic tubes since ceramics are successfully used in CB industrial processes [33]. The kinetic model presented in this paper gave consistent results that were validated from experiments. The kinetic code predicts the chemical conversion as a function of residence time for given conditions of temperature, pressure, and feed gas flow-rates. Thus, it can be used as a design tool during reactor scaling-up. For example, the required residence time to obtain a complete chemical conversion is a key parameter that determines the dimension of the reaction zone.

5. Conclusion

Kinetic simulation of methane dissociation in various experimental conditions was carried out with the Dsmoke software. The kinetic model predictions agreed with the general sequence of decomposition: a stepwise dehydrogenation with the successive intermediates C_2H_6, C_2H_4, and C_2H_2. Nevertheless, other compounds were also involved as chemical intermediates whatever the temperature. Simulations with various natural gas compositions showed small difference in CH_4 conversion after 1 ms. A global kinetic expression for the overall dissociation reaction was identified from the reactor model ($k_0 = 6.6 \times 10^{13}\ s^{-1}$ and $E_a = 370$ kJ/mol), assuming a plug-flow and non-catalytic reaction.

The 10 kW solar experimental reactor was modelled by three plug-flow reactors in series to take into account the temperature profile in the different zones of the reactor tubes (pre-heating, isothermal, cooling). The model shows reasonably good agreement with experimental results, especially for CH_4 conversion, and mole fractions of CH_4 and H_2. It also confirms the importance of residence time and temperature in order to reach high conversion. Moreover, the formation of CB occurs later than H_2 formation and the production of PAHs as intermediate products is identified. Although the kinetic model is limited in terms of particle diameters (60 nm as the upper value), it proved to be a valuable and accurate calculation code in the field of thermal methane dissociation.

Acknowledgements

This study was funded by the European Project Solhycarb (FP6, Contract SES-CT2006-19770). The authors wish to thank J.L. Sans, M. Garrabos, and O. Prévost for their contribution to experimental results.

References

[1] M. Momirlan, T.N. Veziroglu, Current status of hydrogen energy, Renew. Sustain. Energy Rev. 6 (1–2) (2002) 141–179.
[2] P. Spath, M. Mann, Life cycle assessment of hydrogen production via natural gas steam reforming, Technical Report NREL/TP-570-27637, NREL 2000.
[3] M. Kogan, A. Kogan, Production of hydrogen and carbon by solar thermal methane splitting. I. The unseeded reactor, Int. J. Hydrogen Energy 28 (11) (2003) 1187–1198.
[4] J.K. Dahl, K.J. Buechler, A.W. Weimer, A. Lewandowski, C. Bingham, Solar-thermal dissociation of methane in a fluid-wall aerosol flow reactor, Int. J. Hydrogen Energy 29 (7) (2004) 725–736.
[5] D. Hirsch, A. Steinfeld, Solar hydrogen production by thermal decomposition of natural gas using a vortex-flow reactor, Int. J. Hydrogen Energy 29 (1) (2004) 47–55.
[6] D. Trommer, D. Hirsch, A. Steinfeld, Kinetic investigation of the thermal decomposition of CH_4 by direct irradiation of a vortex-flow laden with carbon particles, Int. J. Hydrogen Energy 29 (6) (2004) 627–633.
[7] A. Kogan, M. Kogan, S. Barak, Production of hydrogen and carbon by solar thermal methane splitting. II. Room temperature simulation tests of seeded solar reactor, Int. J. Hydrogen Energy 29 (12) (2004) 1227–1236.
[8] J.K. Dahl, K.J. Buechler, R. Finley, T. Stanislaus, A.W. Weimer, A. Lewandowski, C. Bingham, A. Smeets, A. Schneider, Rapid solar-thermal dissociation of natural gas in an aerosol flow reactor, Energy 29 (5–6) (2004) 715–725.
[9] P.V. Zedtwitz, J. Petrasch, D. Trommer, A. Steinfeld, Hydrogen production via the solar thermal decarbonization of fossil fuels, Sol. Energy 80 (10) (2006) 1333–1337.
[10] S. Abanades, G. Flamant, Hydrogen production from solar thermal dissociation of methane in a high-temperature fluid-wall chemical reactor, Chem. Eng. Process.: Process Intensif. 47 (3) (2008) 490–498.
[11] M.H. Back, R.A. Back, Thermal decomposition and reactions of methane, in: L.F. Albright, B.L. Crynes, W.H. Corcoran (Eds.), Pyrolysis. Theory and Industrial Practice, Academic Press, Inc., New York, 1983, pp. 1–24.
[12] O. Olsvik, O.A. Rokstad, A. Holmen, Pyrolysis of methane in the presence of hydrogen, Chem. Eng. Technol. 18 (1995) 349–358.
[13] F. Billaud, G. Guéret, J. Weill, Thermal decomposition of pure methane at 1263 K. Experiments and mechanistic modelling, Thermochim. Acta 211 (1992) 303–322.
[14] J. Happel, L. Kramer, Acetylene and hydrogen from the pyrolysis of methane, Ind. Eng. Chem. 59 (1) (1967) 39–71.
[15] F. Billaud, F. Baronnet, E. Freund, C. Busson, J. Weill, Thermal decomposition of methane: bibliographic study and proposal of a mechanism, Rev. Inst. Fr. Pét. 44 (6) (1989) 813–823.
[16] J. Gonzalez-Aguilar, I. Dème, L. Fulcheri, G. Flamant, T.M. Gruenberger, B. Ravary, Comparison of simple particle–radiation coupling models applied on a plasma black process, Plasma Chem. Plasma Process. 24 (4) (2004) 603–623.
[17] A. Holmen, O.A. Rokstad, A. Solbakken, High-temperature pyrolysis of hydrocarbons. 1. Methane to acetylene, Ind. Eng. Chem.: Process Des. Dev. 15 (3) (1976) 439–444.

[18] J.K. Dahl, V.H. Barocas, D.E. Clough, A.W. Weimer, Intrinsic kinetics for rapid decomposition of methane in an aerosol flow reactor, Int. J. Hydrogen Energy 27 (4) (2002) 377–386.
[19] J.K. Dahl, A.W. Weimer, W.B. Krantz, Sensitivity analysis of the rapid decomposition of methane in an aerosol flow reactor, Int. J. Hydrogen Energy 29 (1) (2004) 57–65.
[20] User's Manual Dsmoke Program, Release 6.0, CMIC Politecnico di Milano, 2006.
[21] E. Ranzi, T. Faravelli, P. Gaffuri, A. Sogaro, Low-temperature combustion: Automatic generation of primary oxidation reactions and lumping procedures, Combust. Flame 102 (1–2) (1995) 179–192.
[22] C. Bruno, F. Cuoco, CH_4 fuel steam reforming for enhanced propulsion performance, in: Proceedings of the International Symposium on Air Breathing Engines, 15th, Bangalore, India, 2001.
[23] M. Falcitelli, S. Pasini, L. Tognotti, Modelling practical combustion systems and predicting NO_x emissions with an integrated CFD based approach, Comput. Chem. Eng. 26 (9) (2002) 1171–1183.
[24] H. Richter, S. Granata, W.H. Green, J.B. Howard, Detailed modeling of PAH and soot formation in a laminar premixed benzene/oxygen/argon low-pressure flame, Proc. Combust. Inst. 30 (2005) 1397–1405.
[25] S. Granata, F. Cambianica, S. Zinesi, T. Faravelli, E. Ranzi, Detailed kinetic of PAH and soot formation in combustion processes: analogies and similarities in reaction classes, in: Proceedings of the European Combustion Meeting, Belgium, 2005.
[26] A. Holmen, O. Olsvik, O.A. Rokstad, Pyrolysis of natural gas: chemistry and process concepts, Fuel Process. Technol. 42 (2–3) (1995) 249–267.
[27] K. Ledjeff-Hey, J. Roes, R. Wolters, CO_2-scrubbing, methanation as purification system for PEFC, J. Power Sources 86 (1–2) (2000) 556–561.
[28] S. Abanades, G. Flamant, High-temperature solar chemical reactors for hydrogen production from natural gas cracking, Chem. Eng. Commun. 195 (9) (2008) 1159–1175.
[29] E.R.G. Eckert, R.M. Drake, Analysis of Heat and Mass Transfer (1987) 336–337.
[30] J.R. Fincke, R.P. Anderson, T.A. Hyde, B.A. Detering, Plasma pyrolysis of methane to hydrogen and carbon black, Ind. Eng. Chem. Res. 41 (6) (2002) 1425–1435.
[31] N. Muradov, Hydrogen via methane decomposition: an application for decarbonization of fossil fuels, Int. J. Hydrogen Energy 26 (11) (2001) 1165–1175.
[32] S. Abanades, G. Flamant, Experimental study and modeling of a high-temperature solar chemical reactor for hydrogen production from methane cracking, Int. J. Hydrogen Energy 32 (10–11) (2007) 1508–1515.
[33] J.B. Donnet, R.C. Bansal, M.J. Wang, Carbon Black, 2nd ed., Marcel Dekker, New York, 1993.